Chemical Science

ROYAL SOCIETY OF CHEMISTRY

EDGE ARTICLE

View Article Online
View Journal | View Issue

Cite this: *Chem. Sci.*, 2022, **13**, 5741

All publication charges for this article have been paid for by the Royal Society of Chemistry

Received 30th March 2022
Accepted 19th April 2022

DOI: 10.1039/d2sc01832b

rsc.li/chemical-science

Aqueous electrochemically-triggered atom transfer radical polymerization†

Boyu Zhao, Fred Pashley-Johnson, Bryn A. Jones and Paul Wilson *

Simplified electrochemical atom transfer radical polymerization (seATRP) using Cu^{II}–*N*-propyl pyridineimine complexes ($Cu^{II}(NPPI)_2$) is reported for the first time. In aqueous solution, using oligo(ethylene glycol) methyl ether methacrylate (OEGMA), standard electrolysis conditions yield POEGMA with good control over molecular weight distribution ($Đ_m$ < 1.35). Interestingly, the polymerizations are not under complete electrochemical control, as monomer conversion continues when electrolysis is halted. Alternatively, it is shown that the extent and rate of polymerization depends upon an initial period of electrolysis. Thus, it is proposed that seATRP using $Cu^{II}(NPPI)_2$ follows an electrochemically-triggered, rather than electrochemically mediated, ATRP mechanism, which distinguishes them from other $Cu^{II}L$ complexes that have been previously reported in the literature.

Introduction

Electrochemical intervention in synthesis and catalysis has received renewed interest over the last 5–10 years.[1–6] From a synthetic point of view, the use of an applied potential/current enables accurate control over the thermodynamics and/or kinetics of electron transfer processes.[7,8] This can enhance the selectivity of chemical transformations and confer spatiotemporal control over synthetic and catalytic reactions of small and macromolecular organic molecules/polymers, amongst others.

In the context of reversible deactivation radical polymerization (RDRP) electrochemical intervention has been employed to regulate polymer synthesis through control of the dynamic equilibrium between dormant and active (radical) species which allows the overall radical concentration to be accurately controlled.[9–11,53] In atom transfer radical polymerization (ATRP)[12,13] the equilibrium (K_{ATRP}) is between a dormant alkyl (R–X) or macromolecular (P_n–X) halide and propagating radicals ($R^{\bullet}/P_n^{\bullet}$) which undergo reversible redox reactions with transition metal complexes.

In 2011, Matyjaszewski and co-workers showed that the redox nature of the Cu-mediated ATRP mechanism could lend itself to electrochemical manipulation and control.[10] The active, yet oxidatively labile $Cu^{I}L$ complex was formed *in situ* when a reducing potential (E_{app}) was applied at the working electrode (WE) to induce a one electron reduction of an inactive $Cu^{II}L$ precursor. Activation of the dormant species (R–X/P_n–X) in the reaction media then generated the radical species ($R^{\bullet}/P_n^{\bullet}$), and the Cu-complex in a higher oxidation state (X–$Cu^{II}L$). Well controlled polymerization of methyl acrylate was reported suggesting that the deactivation step of the equilibrium, between the propagating radical ($P_n^{\bullet}$) and X–$Cu^{II}L$, reforming the dormant species (P_n–X) and $Cu^{I}L$ respectively, was not perturbed by the electrochemical intervention. In fact, it was shown that by switching the E_{app} at the WE to an oxidizing potential the polymerization could be completely switched off, conferring high fidelity on-off spatiotemporal control over polymer synthesis in solution.

In the 10 years since this discovery, eATRP has been employed for the synthesis of polymers with a variety of compositions and architectures including block copolymers, bioconjugates, star and graft (co)polymers.[14–22] It is compatible with aqueous[23,24] and organic[10] media whilst heterogeneous systems such mini-emulsion[25–28] and surface-initiated (si-eATRP)[29–32] polymerizations have also been reported. Furthermore, the complex reaction set-up, initially involving a 3-electrode divided electrochemical cell, has been simplified by the use of sacrificial counter electrodes (typically Al-wire), enabling undivided cells to be used in either 3-electrode (potential controlled) or 2-electrode (current controlled) configurations giving rise to simplified electrochemical atom transfer radical polymerisaiton (seATRP).[33] This development is significant as it enables the chemistry to be performed using commercial, standardized hardware.[24]

The most widely studied systems for aqueous eATRP employ $Cu^{II}X$ salts with tetradentate ligands *tris*(2-(dimethylamino) ethyl)amine (Me_6-Tren)[10,34,35] or *tris*(2-pyridylmethyl)amine (TPMA).[33,36,37] They form more active complexes, having high K_{ATRP} values.[38] The ligands stabilize Cu^{II} more than Cu^{I} with cyclic voltammetry (CV) indicating that $Cu^{I}Me_6$-Tren and Cu^{I}TPMA are strongly reducing complexes, leading to fast activation (k_{act}) of R–X/P_n–X.[39,40] The k_{act} (and K_{ATRP}) can

University of Warwick, UK. E-mail: p.wilson.1@warwick.ac.uk

† Electronic supplementary information (ESI) available. See https://doi.org/10.1039/d2sc01832b

increase by orders of magnitude when aqueous media is employed, which in the absence of appropriate conditions and/or external control of active catalyst generation, can result in high radical concentrations which has a detrimental effect on the polymerization.[41,42] A great deal of discovery and optimization, of which eATRP is one example, has resulted in the development of efficient, well controlled aqueous ATRP reactions using these highly active complexes.[9,43]

Prior to this, less active complexes composed of bidentate ligands such as bipyridine (bpy) and *N*-alkyl pyridine imines (NAPI) were more suitable for aqueous ATRP.[44–49] They stabilize Cu^{I} more than Cu^{II}, form less reducing Cu^{I} complexes and have lower k_{act} and K_{ATRP} leading to lower radical concentrations. On one hand, this means that larger catalyst concentrations are required to mediate well controlled ATRP. On the other hand, it can also be beneficial for polymerizations carried out in aqueous media wherein increased k_{act} and K_{ATRP} can lead to higher radical concentrations when more active complexes are employed. For example, 20 years ago, Haddleton and Perrier described in detail the efficient, well controlled polymerization of oligo(ethylene glycol) methyl ether methacrylate (OEGMA) using $Cu^{I}(NAPI)_2$ complexes in water.[44–46] The rates of reaction and control over the polymerization were optimized with respect to $[Cu^{I}(NAPI)_2]/[Cu^{II}(NAPI)_2]$ which was controlled from the outset by using known amounts of $Cu^{I}Br$ and $Cu^{II}Br_2$ to form a mixed complex system. To accurately achieve the target $[Cu^{I}(NAPI)_2]/[Cu^{II}(NAPI)_2]$ ratio's careful handling of oxidatively labile Cu^{I} complexes and thoroughly deoxygenated reaction conditions were required. Looking back at this work, we considered the possibility of controlling $[Cu^{I}(NAPI)_2]/[Cu^{II}(NAPI)_2]$ electrochemically, thus avoiding the need to handle the oxidatively labile Cu^{I} complexes. There are currently no reports of eATRP using $Cu(NAPI)_2$ complexes, in either organic or aqueous media in the literature. We were inspired to investigate these complexes with a view to mediate eATRP at less reducing potentials and currents. Long term, we hope this will help to overcome some of the initial limitations associated with oxygen reduction (at more reducing potentials) in our related work in scanning electrochemical probe directed eATRP.[50]

To this end, herein we report for the first time the use of the *N*-propyl pyridineimine (NPPI) ligand to form $Cu^{II}(NPPI)_2$ complexes for eATRP of $OEGMA_{300}$. Well controlled polymerization ($Đ_m \approx 1.30$) is possible and initial investigations into the mechanism suggest that an alternative electrochemically-triggered process is prevalent for these less-active copper complexes.

Results and discussion

Comparative CV of $Cu^{II}L$ complexes; Cu^{II}TPMA, $Cu^{II}Me_6$Tren and $Cu^{II}(NPPI)_2$ were initially performed in solutions of the reaction mixture (10% (v/v) $OEGMA_{300}$ in H_2O) in the absence and presence of the initiator, hydroxyethyl-2-bromoisobutyrate (HEBiB) (Fig. S1–S3†). In the absence of HEBiB, each complex exhibited the $[Cu^{II}L]/[Cu^{I}L]$ redox process and as expected the standard reduction potential ($E^{\theta} \approx E_{1/2} = E_{pc} + E_{pa}/2$) shifted to less reducing potentials (*vs.* Ag/AgCl) going from $Cu^{II}Me_6$Tren ($E_{1/2} = -0.40$ V) to Cu^{II}TPMA ($E_{1/2} = -0.21$ V) to $Cu^{II}(NPPI)_2$ ($E_{1/2} = +0.02$ V) respectively. In the presence of HEBiB the voltammograms of the $Cu^{II}Me_6$Tren and Cu^{II}TPMA complexes show a coupled increase in the cathodic current intensity (E_{pc}) and decrease in the anodic current intensity (E_{pa}). This is indicative of electrochemical reduction of $Cu^{II}L$ to $Cu^{I}L$ followed by fast activation of HEBiB by the $Cu^{I}L$ on the timescale of the CV (0.1 V s^{-1}). In the case of $Cu^{II}(NPPI)_2$ the coupled change in E_{pc} and E_{pa} was not observed. The currents decrease in both the cathodic and anodic scan suggesting that although the presence of HEBiB has an effect on the kinetics of electron transfer, the activation of HEBiB by $Cu^{I}(NPPI)_2$ is slow on the timescale of the CV. These results are in agreement with the literature that suggests that with respect to k_{act}, complexes with Me_6Tren > TPMA ≫ NPPI.[35,38]

Potentiostatic seATRP reactions using each complex were performed in undivided cells using an IKA ElectraSyn device. A commercial Pt-coated electrode (IKA) was employed as the cathode (WE), the anode (CE) was Al-wire and the reference electrode (RE) was Ag^{+}/AgCl. For the bidentate NPPI ligand a ratio of $[OEGMA_{300}] : [HEBiB] : [CuBr_2] : [NPPI] = [20] : [1] : [0.5] : [1.25]$ was used. When $E_{app} = E_{1/2} = +0.02$ V the resistance in the system was too high preventing the IKA ElectraSyn from operating. However, when an overpotential of 60 mV was applied ($E_{app} = -0.04$ V) polymerization was complete within 2 h yielding $POEGMA_{300}$ with $M_{n,SEC} = 9200$ g mol^{-1} and $Đ_m = 1.31$ (Table 1, entry 1, Fig. S4†).

Table 1 seATRP of $OEGMA_{300}$ in H_2O. $[OEGMA_{300}] : [HEBiB] : [CuBr_2] : [NPPI] = [20] : [1] : [0.5] : [1.25]$; room temperature[a]

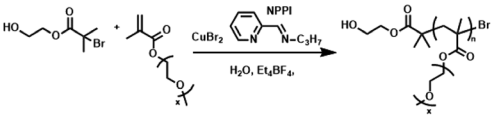

Entry	E_{app}/V	Time/h	Conv[k]	$M_{n,th}$[l]/g mol^{-1}	$M_{n,SEC}$[m]/g mol^{-1}	$Đ_m$[m]
1	−0.04	2	100%	6211	9200	1.31
2	−0.08	2	96%	5971	11 000	1.30
3	−0.12	2	96%	6211	12 800	1.29
4	−0.16	2	99%	6211	10 200	1.32
5[b]	−0.16	2	100%	6211	10 000	1.28
6[c]	−0.16	2	100%	6211	9000	1.26
7[d]	−0.16	2	96%	5971	18 200	1.50
8[e]	−0.16	2	67%	4231	21 800	1.98
9[f]	−0.16	2	96%	9811	14 600	1.30
10[g]	−0.16	6.5	67%	14 951	14 900	1.23
11[h]	−0.16	2	98%	3151	7800	1.31
12[i]	−0.16	2	90%	11 011	14 000	1.33
13[j]	−0.16	2	95%	23 011	21 500	1.33

[a] $[Cu^{II}Br_2] = 8.8$ mM. [b] $[OEGMA_{300}] = 20\%$ v/v. [c] $[OEGMA_{300}] = 30\%$ v/v. [d] $[Cu^{II}Br_2] = 4.4$ mM. [e] $[Cu^{II}Br_2] = 2.2$ mM. [f] $OEGMA_{500}$ used. [g] $OEGMA_{1100}$ used. [h] $[M]/[I] = 10$. [i] $[M]/[I] = 40$. [j] $[M]/[I] = 80$. [k] Determined *via* ^{1}H NMR of reaction samples performed in D_2O. [l] $M_{n,th} = [(\text{conv.}/100 \times DP_{n,th})\ x\ 300/500(e)/1100(f)] + 211$. [m] From THF SEC.

When Me_6Tren and TPMA were employed as ligands ([$OEGMA_{300}$] : [HEBiB] : [$CuBr_2$] : [L] = [20] : [1] : [0.5] : [0.6]), $E_{app} = E_{1/2}$ was sufficient for the ElectraSyn to operate. In both cases, conversions were limited to <80% after 4 h and the control over the polymerization was poor ($Đ_m$ > 4, Table S1†). This is likely due to the stoichiometry of $Cu^{II}Br_2$ employed which equates to [$Cu^{II}Br_2$] = 8.8 mM. Although, this is suitable for the less active Cu^{II}/NPPI system, it is much higher than is required for the so-called highly active complexes leading to higher than necessary [Cu^{I}L] and [$R^{\bullet}/P_n^{\bullet}$] due to rapid over activation when $E_{app} = E_{1/2}$ which ultimately compromises the outcome of the polymerization.

Incrementally increasing the overpotential by 40 mV had little effect on the rate of the polymerization with conversions remaining high (>95%), and control being retained with $Đ_m \approx$ 1.30 (Table 1, entries 2–4, Fig. S5–S7†). The E_{app} was then fixed at −0.16 V and [$OEGMA_{300}$] was increased to 20% and 30% v/v respectively (Table 1, entries 5–6). There was no significant change in the control over the polymerization with low dispersities ($Đ_m$ < 1.30) obtained (Fig. S8 and S9†). Kinetic analysis showed that quantitative conversions were obtained with 2 h. However, the semi-log plot showed that whilst the pseudo first order kinetics were observed at [$OEGMA_{300}$] = 10% v/v, distinct deviations were apparent at the higher concentrations (Fig. S10†). The observed increase in rate throughout the reaction is in agreement with Haddleton and Perrier who attributed it to water and monomer completing with the ligand for coordination at the Cu centre thus affecting the Cu^{II}/Cu^{I} equilibrium.[44] With this in mind, the remaining reactions were performed at [$OEGMA_{300}$] = 10% v/v.

Decreasing the [Cu] from 8.8 mM to 4.4 mM and 2.2 mM had a detrimental effect on the control over the polymerization ($Đ_m$ > 1.50, Table 1, entries 7–8). Increasing the length of the OEGMA monomer using $OEGMA_{500}$ and $OEGMA_{1100}$ had little effect on the control over the polymerization, with low dispersities retained ($Đ_m$ < 1.30, Fig. S11 and S12†), though the rate of polymerization for $OEGMA_{1100}$ was slower than $OEGMA_{300/500}$ reaching 67% within 6.5 h (Table 1, entries 9–10).

Under the conditions established above (E_{app} = −0.16 V; [M] = 10% v/v), the $DP_{n,th}$ was varied such that [M] : [I] = [10]/[20]/[40]/[80] : [1]. The polymerizations reached 90–98% conversion within 2 h, proceeding with good control over M_n and dispersity ($Đ_m$ < 1.35; Table 1, entries 4, 11–13). An overlay of the SEC chromatograms shows the expected shift in the narrow molecular weight distributions to higher molecular weights as a function of [M]/[I] (Fig. 1A). A plot of $M_{n,SEC}$ *vs.* [M]/[I] indicates

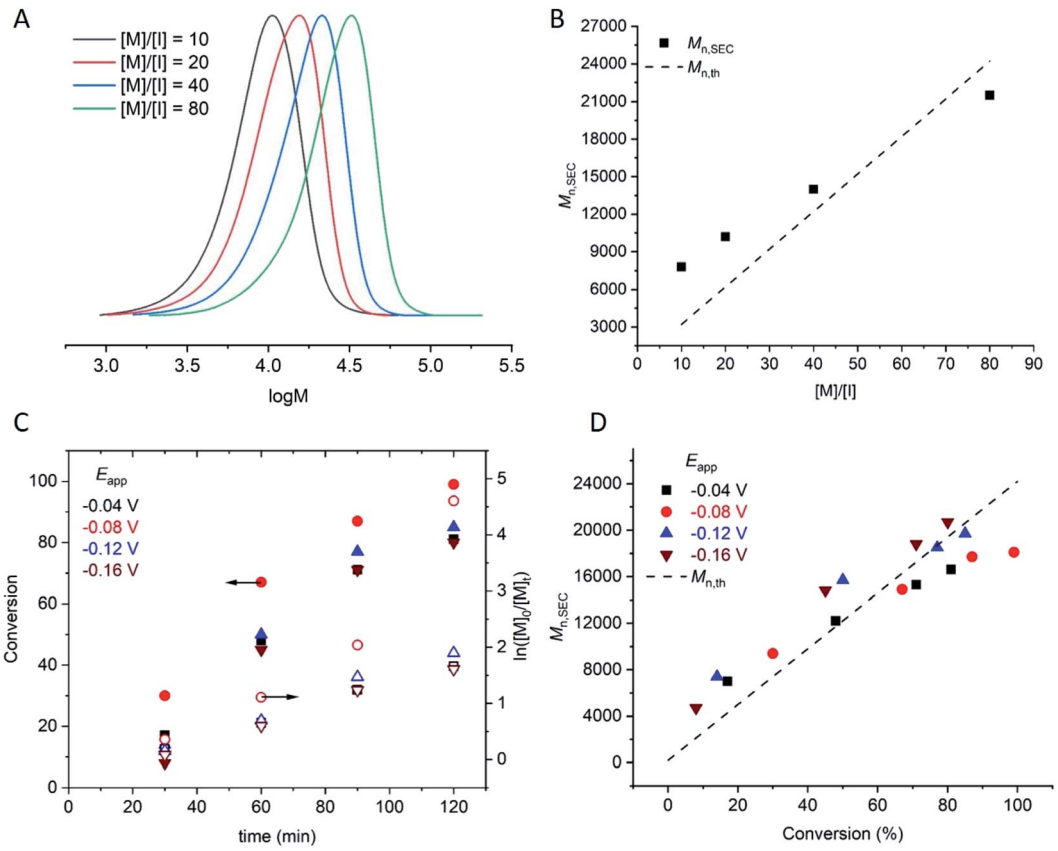

Fig. 1 For seATRP of [$OEGMA_{480}$] : [HEBiB] : [$CuBr_2$] : [NPPI] = [M] : [1] : [0.5] : [1.25]; (A) SEC in THF showing a shift in molecular weight distributions as for [M] = 10, M_n = 7800 g mol^{-1}, $Đ_m$ = 1.31; [M] = 20, M_n = 10 200 g mol^{-1}, $Đ_m$ = 1.32, [M] = 40, M_n = 14 000 g mol^{-1}, $Đ_m$ = 1.33, [M] = 80, M_n = 21 500 g mol^{-1}, $Đ_m$ = 1.33. (B) Plot of $M_{n,SEC}$ as a function of [M]/[I] for [M] = 10, 20, 40, 80, [I] = 1, (E_{app} = −0.16 V). (C) Conversion and pseudo first order kinetic plots as a function of E_{app}. (D) Evolution of the $M_{n,SEC}$ with conversion during polymerizations performed at different E_{app} ([M]/[I] = 80).

a linear increase in $M_{n,SEC}$ as a function of [M]/[I], with slight deviations in $M_{n,SEC}$ and $M_{n,th}$ converging as [M]/[I] increased (Fig. 1B).

Kinetic analyses of the polymerizations performed with [M] : [I] = [80] : [1] revealed that the apparent rate constant for propagation was k_p^{app} = 0.0167 min^{-1} at E_{app} = −0.04 V (Fig. 1C). Initially, more reducing potentials (E_{app} = −0.08 V) resulted in a small increase in the rate of polymerization (k_p^{app} = 0.0456 min^{-1}). However, at higher overpotentials (E_{app} = −0.12 V, −0.16 V), the rate decreased back to k_p^{app} = 0.0201 min^{-1} and 0.0174 min^{-1} respectively. At these potentials, E_{app} is close to E_{pc} at which point the reduction of Cu^{II}/L to Cu^{I}/L is not governed by the electrode potential and is limited by the rate of diffusion of accumulated Cu/L species to and from the electrode surface to and from the bulk. Irrespective of E_{app}, a linear increase in $M_{n,SEC}$ as a function of conversion was observed with good agreement with the theoretical molecular weight ($M_{n,th}$) (Fig. 1D).

A hallmark of eATRP is the temporal control conferred by switching the potential/current on and off. At reducing potentials Cu^{II}/L is reduced to Cu^{I}/L leading to activation of dormant chains which can undergo propagation and subsequent deactivation events *via* the proposed ATRP mechanism. If the potential is switched off, or an oxidising potential is applied, reduction of Cu^{II}/L nolonger occurs so activation of the dormant chains stops and the polymerization is halted. Conducting this experiment using [$OEGMA_{300}$] : [HEBiB] : [$CuBr_2$] : [NPPI] = [20] : [1] : [0.5] : [1.25] and applying E_{app} = −0.16 V ([M] = 10% v/v), conversion reached >50% within 20 min (Fig. 2). The potential was then switched off (E_{app} = 0 V) and stirring was continued for a further 20 min, after which conversion unexpectedly increased to >80%. The polymerization reached >90% conversion through an additional 'on' (20 min) and 'off' (20 min) cycle, indicating that Cu^{II}(NPPI)$_2$ lacked the temporal control associated with eATRP. The lack of temporal control with this less active catalyst system is in agreement with reported differences in temporal control related to catalyst activity observed in photo-ATRP.[51]

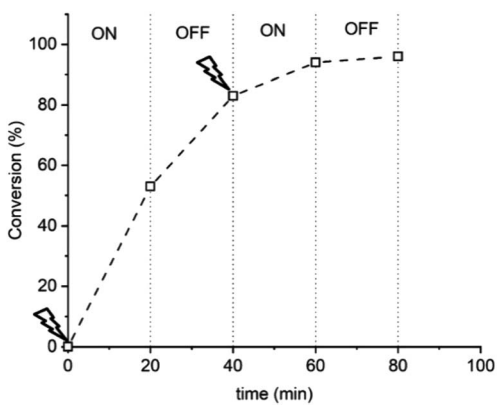

Fig. 2 Conversion *vs.* time plot demonstrating a lack of temporal control afforded by seATRP with [$OEGMA_{300}$] : [HEBiB] : [$CuBr_2$] : [NPPI] = [20] : [1] : [0.5] : [1.25] : [0.15]; E_{app} = −0.16 V.

Unlike in eATRP reactions using Cu^{II}(Me_6Tren) and Cu^{II}(TPMA) complexes, it was observed that the reaction solutions containing Cu^{II}(NPPI)$_2$ changed colour, from green to brown, during electrolysis (Fig. S14†). The brown colour resembled that reported in early aqueous ATRP using Cu^{I}(NAPI)$_2$ complexes.[44–46] Thus, it was hypothesized that the overpotentials applied and the less activating nature of the Cu^{I}(NPPI)$_2$ complex, resulted in accumulation of stable Cu^{I}(NPPI)$_2$ in the reaction media which was capable of continuing to mediated the polymerization of OEGMA when E_{app} was removed.

To explore this hypothesis, the temporal control experiment was repeated using [$OEGMA_{300}$] : [HEBiB] : [$CuBr_2$] : [NPPI] = [20] : [1] : [0.5] : [1.25]. After the electrolysis period (E_{app} = −0.08 V; $t_{E_{app}}$ = 30 min), the reaction solution was brown, indicative of Cu^{I}(NPPI)$_2$ accumulation, and conversion had reached 33% (Fig. S15A†). Concurrently, electrolysis was stopped and sparging with compressed air was commenced to rapidly introduce O_2 into the reaction solution to stop the polymerization. The solution quickly changed colour from brown to green, indicative of oxidation of Cu^{I}(NPPI)$_2$ to Cu^{II}(NPPI)$_2$ and no further conversion was observed (Fig. S15B†). In an attempt to re-initiate the polymerization, the reaction solution was sparged for second time, this time with N_2 to displace the O_2 previously added to the solution, prior to a second period of electrolysis. Pleasingly, re-initiation was observed (E_{app} = −0.08 V; $t_{E_{app}}$ = 30 min) with the polymerization reaching 64% conversion (Fig. S15C†), yielding $POEGMA_{300}$ with $M_{n,SEC}$ = 9800 g mol^{-1} and $Đ_m$ = 1.25 (Fig. S16†) which is comparable to the $POEGMA_{300}$ obtain during the constant electrolysis reactions.

A series of experiments was then performed in which reaction solutions ([$OEGMA_{300}$] : [HEBiB] : [$CuBr_2$] : [NPPI] = [20] : [1] : [0.5] : [1.25]) were electrolyzed at constant potential (E_{app} = −0.08 V) for increasing periods of time ($t_{E_{app}}$ = 5, 10, 20, 30 min) before the potential was removed (E_{app} = 0 V). Samples were taken for analysis after electrolysis and at regular intervals after the potential was removed. Increasing the initial electrolysis times led to an increase in initial conversion from 2% (E_{app} = −0.08 V; $t_{E_{app}}$ = 5 min) to 22% (E_{app} = −0.08 V; $t_{E_{app}}$ = 30 min). In all experiments monomer conversion continued upon removal of E_{app} (Fig. 3A). At shorter electrolysis times, conversion continued up to a total reaction time of 60 min resulting in final conversions of 18% and 35% when $t_{E_{app}}$ = 5 and 10 min respectively. Increasing the initial electrolysis time to 20 min yielded initial conversions of 11% with monomer conversion continuing thereafter to reach a final conversion of 56% after a total reaction time of 70 min. When the reaction solution was electrolyzed for 30 min monomer conversion continued for a total reaction time of 90 min, reaching 93% conversion. Kinetic analysis of these reactions revealed that the rate of the reaction also increased from k_p^{app} = 0.0028 min^{-1} when $t_{E_{app}}$ = 5 min to k_p^{app} = 0.0425 min^{-1} when $t_{E_{app}}$ = 30 min (Fig. 3B). An overlay of the SEC chromatograms shows that the polymerization continues after the initial electrolysis period with the molecular weight distributions shifting to higher molecular weights as a function of time (Fig. 3C). The final polymer

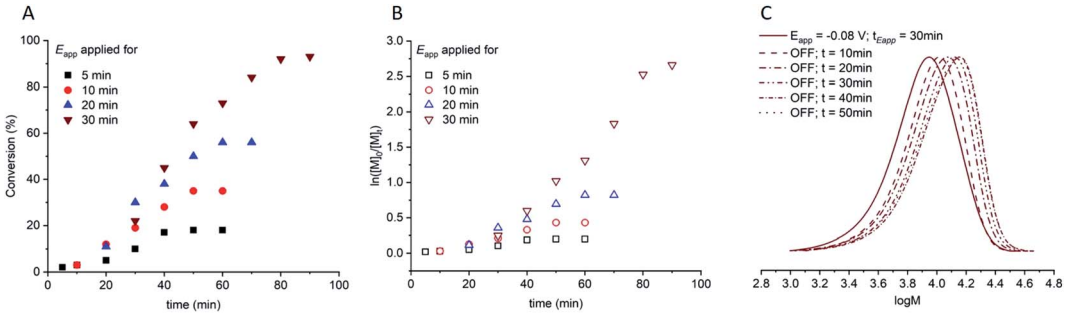

Fig. 3 For triggered seATRP of [$OEGMA_{300}$] : [HEBiB] : [$CuBr_2$] : [NPPI] = [20] : [1] : [0.5] : [1.25]; (A) conversion *vs.* time plot for polymerizations with different $t_{E_{app}}$. (B) Pseudo first order kinetic plots for polymerizations for $t_{E_{app}}$ = 5 min, k_p^{app} = 0.0028 min^{-1}; $t_{E_{app}}$ = 10 min, k_p^{app} = 0.0046 min^{-1}; $t_{E_{app}}$ = 20 min, k_p^{app} = 0.0218 min^{-1}; $t_{E_{app}}$ = 30 min, k_p^{app} = 0.0425 min^{-1}. (C) SEC in THF showing the evolution of the molecular weight distribution after electrolysis (E_{app} = −0.08 V, $t_{E_{app}}$ = 30 min, solid line) and at 10 minutes intervals after the potential was removed (E_{app} = 0 V, dashed lines, final $M_{n,SEC}$ = 9300 g mol^{-1}, $Đ_m$ = 1.33).

obtained (E_{app} = −0.08 V; $t_{E_{app}}$ = 30 min) was comparable to the polymer obtained by uninterrupted electrolysis (Table 1; entry 2) with $M_{n,SEC}$ = 9300 g mol^{-1} and $Đ_m$ = 1.33.

Quantification of the end group fidelity using conventional ^{1}H NMR analysis was not possible as poly(methacrylates) do not contain an ω-methine proton to integrate against signals at the α-chain end. To exemplify end group fidelity, a chain extension experiment was performed. Homopolymerization of $OEGMA_{300}$ was performed using [$OEGMA_{300}$] : [HEBiB] : [$CuBr_2$] : [NPPI] = [20] : [1] : [0.5] : [1.25] (E_{app} = −0.08 V). After electrolysis for 30 min (Table 2, entry 1) and stirring at room temperature in the absence of electrolysis for an additional 90 min near quantitative conversion was obtained (Table 2, entry 2, Fig. S17†). At this point a second aliquot of $OEGMA_{300}$ (1 mL, [$OEGMA_{300}$] : [$POEGMA_{300}$-Br] = [20] : [1]) was added and electrolysis was again applied (E_{app} = −0.08 V) for 30 min (Table 2, entry 3) followed by stirring in the absence of electrolysis for an additional 90 min reaching a final conversion of 81% (Table 2, entry 4). A clear shift in the molecular weight distribution was evident *via* SEC analysis (Fig. 4). The molecular weight of the final $POEGMA_{300}$ obtained ($M_{n,SEC}$ = 16 600 g mol^{-1}) was in reasonable agreement to the theoretical molecular weight ($M_{n,th}$ = 12 200 g mol^{-1}) relative to the homopolymerizations performed. Although this result exemplifies good chain-end fidelity, there is scope for optimization based on a gradual increase in tailing to low molecular weight, which increased during the course of the reaction resulting in a gradual increase in dispersity ($Đ_m$ = 1.27–1.45, Table 2).

The electrochemically triggered reaction conditions were also compatible with polymerizations of $OEGMA_{300}$ targeting higher molecular weights. When $DP_{n,th}$ = 200, the reaction solution was electrolyzed for 30 min (E_{app} = −0.08 V) leading to 13% conversion. The reaction continued in the absence of electrolysis for an additional 90 min, reaching 89% conversion (Fig. S18†) furnishing $POEGMA_{300}$ with relatively low dispersity ($Đ_m$ = 1.32, Fig. S19†). To expand the monomer scope, 2-*N*-morpholinoethyl methacrylate ($DP_{n,th}$ = 200) was electrolyzed for 30 min (E_{app} = −0.08 V) resulting in 40% conversion. The reaction was allowed to continue in the absence of electrolysis for an additional 90 min, reaching 65% conversion (Fig. S20 and S21†).

To explore the mechanism, the polymerization using [$OEGMA_{300}$] : [HEBiB] : [$CuBr_2$] : [NPPI] = [20] : [1] : [0.5] : [1.25] ($t_{E_{app}}$ = 30 min; E_{app} = −0.08 V) was repeated and the electrochemical reduction of $Cu^{II}(NPPI)_2$ to $Cu^{I}(NPPI)_2$ followed by UV-vis spectroscopy (Fig. 5). Prior to electrolysis the reaction solution was green and the characteristic $Cu^{II}(NPPI)_2$ absorbance band was present at λ = 670 nm,

Table 2 Electrochemically triggered seATRP of $OEGMA_{300}$ in H_2O. [$OEGMA_{300}$] : [HEBiB] : [$CuBr_2$] : [NPPI] = [20] : [1] : [0.5] : [1.25]; followed by *in situ* chain extension using $OEGMA_{300}$ (20 eq.); E_{app} = −0.08 V; $t_{E_{app}}$ = 30 min; room temperature[a]

Entry	E_{app}/V	Time/min (t_{total})	Conv[b]	$M_{n,th}$/g mol^{-1}	$M_{n,SEC}$[e]/g mol^{-1}	$Đ_m$[e]
1	−0.08	30 (30)	33%	2191[c]	7300	1.26
2	—	90 (120)	>99%	6211[c]	11 300	1.31
3	−0.08	30 (150)	57%	9631[d]	13 800	1.34
4	—	90 (240)	81%	11 071[d]	16 600	1.45

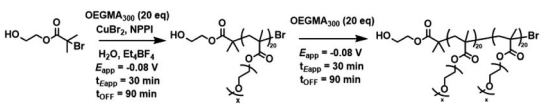

[a] $[Cu^{II}Br_2]$ = 8.8 mM. [b] Determined *via* ^{1}H NMR of reaction samples performed in D_2O. [c] $M_{n,th}$ = [(conv./100 × $DP_{n,th}$) × 300] + 211. [d] $M_{n,th}$ = [(conv./100 × $DP_{n,th}$) × 300] + 6211. [e] From THF SEC.

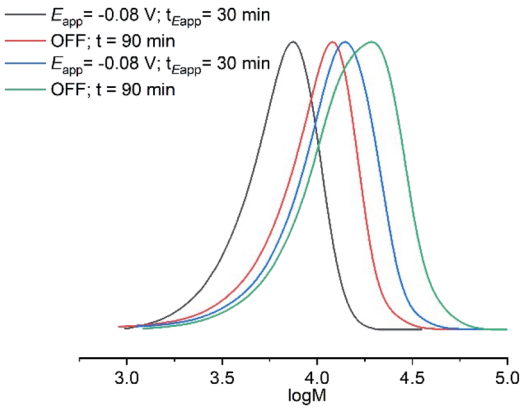

Fig. 4 SEC in THF showing the evolution of the molecular weight distribution during electrochemically triggered eATRP of $OEGMA_{300}$ ([$OEGMA_{300}$] : [HEBiB] : [$CuBr_2$] : [NPPI] = [20] : [1] : [0.5] : [1.25]; E_{app} = −0.08 V; $t_{E_{app}}$ = 30 min) and chain extension ([$OEGMA_{300}$]- : [$POEGMA_{300}$-Br] = [20] : [1]; E_{app} = −0.08 V; $t_{E_{app}}$ = 30 min) (Table 2).

assigned to the d–d transitions of the Cu^{II} centre. After electrolysis the reaction solution was brown in colour, qualitatively confirming the reduction of $Cu^{II}(NPPI)_2$ to $Cu^{I}(NPPI)_2$. UV-vis of the reaction solution immediately after electrolysis showed disappearance of the absorbance band at λ = 670 nm and appearance of a new, strong absorbance band at λ = 465 nm, confirming reduction of $Cu^{II}(NPPI)_2$ to $Cu^{I}(NPPI)_2$. The absorbance at λ = 465 nm was assigned to MLCT between the Cu^{I} centre and the π^* of the surrounding NPPI ligands, as reported for other bipyridyl and/or diimine based complexes of Cu^{I}.[52]

In order to quantify the concentration of $Cu^{I}(NPPI)_2$ present after electrolysis, a calibration plot of $Cu^{I}(NPPI)_2$ was used to determine the molar extinction coefficient of $Cu^{I}(NPPI)_2$ (ε = 1359 M^{-1} cm^{-1}, Fig. S22†). Prior to electrolysis, the concentration of $Cu^{II}(NPPI)_2$ in the reaction solution was 8.8 mM. After electrolysis for 30 min, conversion reached 24% (Fig. 5A) and [$Cu^{I}(NPPI)_2$] was measured and found to be 4.94 mM (Fig. 5B). The reaction was again allowed to continue in the absence of an applied potential (E_{app} = 0 V). Though the polymerization continued, the colour of the reaction solution gradually changed from brown back to green over the course of the reaction. Further UV-vis analysis of the reaction solution allowed [$Cu^{I}(NPPI)_2$] to be followed, revealing a steady decrease over time eventually reaching 1.37 mM after 30 min at which point the reaction had reached 72% conversion.

Identical analyses were performed during polymerization of $OEGMA_{300}$ using Cu^{II}TPMA and $Cu^{II}Me_6$-Tren. Due to the tetradentate nature of TPMA and ME_6-Tren, the reaction solutions were composed of [$OEGMA_{300}$] : [HEBiB] : [$CuBr_2$] : [TPMA/Me_6-Tren] = [20] : [1] : [0.5] : [0.6]. Both Cu^{II}TPMA and $Cu^{II}Me_6$-Tren produced blue solutions prior to electrolysis. Qualitatively, no colour change was observed upon electrolysis. The E_{app} employed was selected based on the $E_{1/2}$ (−0.2 V, TPMA; −0.4 V Me_6-Tren; Fig. S1 and S2†) and electrolysis was initially performed for 30 min before the potential was removed and stirring continued at room temperature. The progress of the reactions was followed by ^{1}H NMR revealing ∼5% conversion after the initial period of electrolysis. UV-vis analysis showed very little change in the absorbance spectra of each complex (Fig. 5C) and unlike the $Cu^{II}(NPPI)_2$ system, no further conversion of monomer to polymer was observed when the reaction was continued for 30 min at E_{app} = 0 V (Fig. 5A). This is perhaps unsurprising considering the relative activity of the Cu^{I}TPMA and $Cu^{I}Me_6$-Tren complexes relative to $Cu^{I}(NPPI)_2$. Thus we repeated the reaction using bipyridine (bipy) to form $Cu^{I}(bipy)_2$ *in situ* which has intermediate activity relative to the highly active complexes derived from Me_6-Tren/TPMA and the less active complex derived from NPPI. Similar to $Cu^{II}(NPPI)_2$, initial conversion in the presence of $Cu^{II}(bipy)_2$ increased with increasing electrolysis time (E_{app} = −0.08 V; $t_{E_{app}}$ = 10–30 min). However, in the absence of electrolysis polymerization was only maintained for 10–20 min reaching only moderate final conversions (< 65%, E_{app} = −0.08 V; $t_{E_{app}}$ = 30 min, Fig. S23†). This suggests that the ability to conduct electrochemically triggered eATRP is directly related to the activity (k_{act} and K_{ATRP}) of the Cu-complex employed.

Overall, these results consolidate the hypothesis that the less activating nature of the $Cu^{I}(NPPI)_2$ complex, and its stability in water results in its accumulation in the reaction media. The accumulated $Cu^{I}(NPPI)_2$ is then capable of mediating the

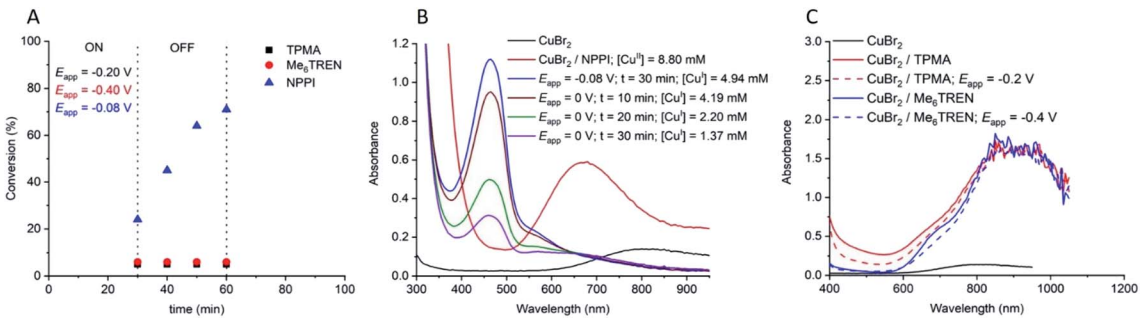

Fig. 5 (A) Conversion *vs.* time plot for seATRP of [$OEGMA_{300}$] : [HEBiB] : [$CuBr_2$] : [L] = [20] : [1] : [0.5] : [L]. For NPPI [L] = [1.25] and for TPMA and Me_6Tren [L] = [0.6] ($t_{E_{app}}$ = 30 min). (B) UV-vis traces showing the reduction of $Cu^{II}(NPPI)_2$ to $Cu^{I}(NPPI)_2$ and the change in [$Cu^{I}(NPPI)_2$] during the triggered seATRP of [$OEGMA_{300}$] : [HEBiB] : [$CuBr_2$] : [NPPI] = [20] : [1] : [0.5] : [1.25]. Using ε = 1359 M^{-1} cm^{-1} [$Cu^{I}(NPPI)_2$] was quantified at each point (see ESI† for calibration and calculation details). (C) UV-vis traces of Cu^{II}(TPMA) and Cu^{II}(Me_6Tren) before and after electrolysis. $E_{app,TPMA}$ = −0.20 V, $E_{app,Me6Tren}$ = −0.40 V, $t_{E_{app}}$ = 30 min.

polymerization of OEGMA when E_{app} was removed. We therefore propose that Cu complexes containing pyridine-imine ligands ($Cu^{II}(NAPI)_2$) follow an electrochemically-triggered, rather than electrochemically mediated, ATRP mechanism wherein E_{app} is only required in order to generate the required $[Cu^{I}(NAPI)_2]$ to initiate and maintain the polymerization reaction.

Finally, to simplify the reaction set up further, current *vs.* time (*I vs. t*) graphs obtained from reactions performed under potentiostatic conditions (Fig. 6A) were used to design a step-wise current profile to enable the electrochemically triggered polymerizations to be performed using a 2-electrode current controlled configuration. Using $[OEGMA_{300}] : [HEBiB] : [CuBr_2] : [NPPI] = [20] : [1] : [0.5] : [1.25]$, a 3-step current profile was initially applied over 30 min ($I_{app} = -3.5$ mA, 8 min; -1.9 mA, 7 min; -0.5 mA, 15 min) resulting in 12% conversion. At this point the reaction continued in the absence of electrolysis for a further 120 min reaching 80% conversion (Fig. S24†) with comparable control ($M_{n,SEC} = 11\,600$ g mol^{-1}; $Đ_m = 1.25$, Fig. 6B) to the polymerizations performed with a potentiostatic trigger. Considering future translation to flow electrolysis, it would be beneficial to trigger these reactions using a single current, truly galvanostatic reaction configuration. With this in mind the reaction was repeated with $I_{app} = -2.0$ mA leading to 16% conversion after the 30 min electrolysis period reaching 95% after a further 120 min stirring in the absence of electrolysis (Fig. S25†). This is very promising for intensification to flow electrolysis, though it should be noted that under these conditions, a higher overall charge is passed during the reaction which has an effect on the outcome of polymerization. Whilst the control respect to the dispersity is retained ($Đ_m = 1.28$, Fig. S26†), the $M_{n,SEC}$ (14 300 g mol^{-1}) and $M_{n,th}$ (6211 g mol^{-1}) diverge relative the potentiostatic and step-wise current profile triggered reactions, leaving scope for optimisation in future. We attribute the divergence in the $M_{n,SEC}$ and $M_{n,th}$ to the gradual increase in the potential (required to maintain I_{app}) during the initial electrolysis period. This leads to an increase in $[Cu^{I}(NPPI)_2]$ and subsequently $[P_n^{\bullet}]$, leading to increased termination and reduced initiator efficiency, relative to the potentiostatic and step-wise current profile triggered polymerizations.

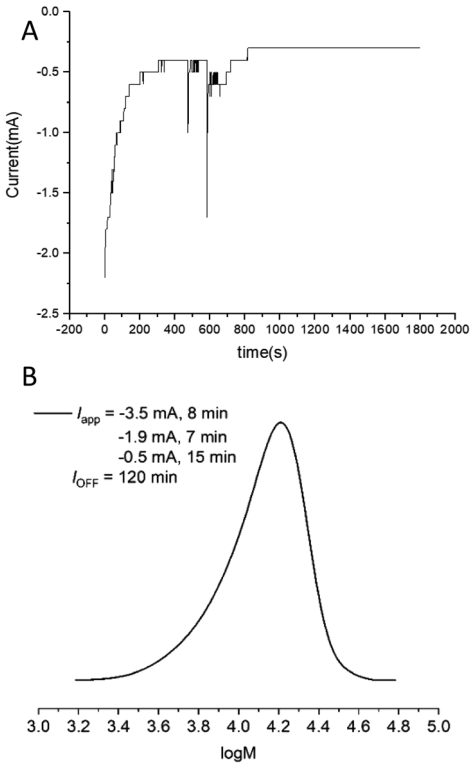

Fig. 6 (A) *I vs. t* plot for the electrochemically triggered seATRP reaction of $OEGMA_{300}$ performed under potentiostatic conditions $[OEGMA_{300}] : [HEBiB] : [CuBr_2] : [NPPI] = [20] : [1] : [0.5] : [1.25]$; $E_{app} = -0.08$ V; $t_{E_{app}} = 30$ min, $Q = 0.78$ C). (B) Molecular weight analysis of the final polymer formed from the same reaction performed using step-wise current profile min ($I_{app} = -3.5$ mA, 8 min; -1.9 mA, 7 min; -0.5 mA, 15 min). SEC in THF $M_{n,SEC} = 11\,600$ g mol^{-1}, $Đ_m = 1.25$.

Conclusions

In summary, seATRP using $Cu(NPPI)_2$ complexes in aqueous solution has been reported for the first time. Typical electrolysis conditions require less reducing potentials ($E_{app} = -0.08$ V) than complexes derived from Me_6-Tren and TPMA. Using $OEGMA_{300}$ as monomer, a range of molecular weights have been targeted with the polymerizations typically complete within 2 h, yielding $POEGMA_{300}$ with good control over the molecular weight distribution ($Đ_m < 1.35$). However, the defining 'on-off' control experiment revealed that the polymerizations were not under complete electrochemical control, as monomer conversion continued in the absence of E_{app}. This is contrary to previous reports using more active $Cu^{II}L$ complexes. Through electrochemically triggered control experiments and UV-vis spectroscopy we have been able to propose that these less activating complexes, that stabilize Cu^{I} more than Cu^{II}, follow an alternative, previously unreported, electrochemically-triggered polymerization pathway. The polymerizations proceed with good control enabling a range of molecular weights to be targeted ($DP_{n,th} = 20$–200). *In situ* chain extension is also possible alluding to potential application to the synthesis of block copolymers. The reaction set-up can also be further simplified to a 2-electrode, galvanostatic configuration which is promising for future intensification through translation to flow electrolysis. However, though suitable for eATRP at reduced catalyst loadings, more active ligands such as Me_6-Tren, TPMA and bipy do not support the electrochemically-triggered polymerization pathway. Indeed, the ability to conduct electrochemically triggered eATRP seems to be directly related to the activity of the Cu-complex and can be related to the k_{act} and K_{ATRP} of the complexes employed. Thus, it is possible that other ligands that stabilize Cu^{I} over Cu^{II} (*e.g.* other substituted NAPI and 1,4-diazabutadiene ligands) could also follow or favour this electrochemically triggered pathway.

Data availability

Experimental procedures and data supporting the research, not presented in the main manuscript, is included in the ESI.† Raw data files are available from the Warwick Research Archive

Portal (WRAP, https://wrap.warwick.ac.uk) and from the corresponding author on request.

Author contributions

Boyu Zhao: investigation; methodology; formal Analysis; validation; visualization; writing – original draft. Fred Pashley-Johnson: investigation; methodology; formal analysis; validation; visualization; writing – original draft. Bryn Jones: Methodology; formal analysis; supervision; writing – review and editing. Paul Wilson: conceptualization; funding acquisition; investigation; methodology; project administration; resources; supervision; writing – review and editing.

Conflicts of interest

There are no conflicts to declare.

Acknowledgements

The authors would like to thank the Polymer Characterization Research Technology Platforms for maintenance and access to facilities. P. W. thanks the Royal Society and Tata companies for the award of a University Research Fellowship (URF\R1\180274).

Notes and references

1 C. Kingston, M. D. Palkowitz, Y. Takahira, J. C. Vantourout, B. K. Peters, Y. Kawamata and P. S. Baran, *Acc. Chem. Res.*, 2020, **53**, 72–83.
2 S. D. Minteer and P. Baran, *Acc. Chem. Res.*, 2020, **53**, 545–546.
3 C. Schotten, T. P. Nicholls, R. A. Bourne, N. Kapur, B. N. Nguyen and C. E. Willans, *Green Chem.*, 2020, **22**, 3358–3375.
4 J. C. Siu, N. Fu and S. Lin, *Acc. Chem. Res.*, 2020, **53**, 547–560.
5 M. Yan, Y. Kawamata and P. S. Baran, *Chem. Rev.*, 2017, **117**, 13230–13319.
6 M. Yan, Y. Kawamata and P. S. Baran, *Angew. Chem., Int. Ed.*, 2018, **57**, 4149–4155.
7 K. D. Moeller, *Chem. Rev.*, 2018, **118**, 4817–4833.
8 C. Sandford, M. A. Edwards, K. J. Klunder, D. P. Hickey, M. Li, K. Barman, M. S. Sigman, H. S. White and S. D. Minteer, *Chem. Sci.*, 2019, **10**, 6404–6422.
9 N. Bortolamei, A. A. Isse, A. J. D. Magenau, A. Gennaro and K. Matyjaszewski, *Angew. Chem., Int. Ed.*, 2011, **50**, 11391–11394.
10 A. J. D. Magenau, N. C. Strandwitz, A. Gennaro and K. Matyjaszewski, *Science*, 2011, **332**, 81–84.
11 Y. Wang, M. Fantin, S. Park, E. Gottlieb, L. Fu and K. Matyjaszewski, *Macromolecules*, 2017, **50**, 7872–7879.
12 P. Chmielarz, M. Fantin, S. Park, A. A. Isse, A. Gennaro, A. J. D. Magenau, A. Sobkowiak and K. Matyjaszewski, *Prog. Polym. Sci.*, 2017, **69**, 47–78.
13 F. Lorandi, M. Fantin, A. A. Isse and A. Gennaro, *Curr. Opin. Electrochem.*, 2018, **8**, 1–7.
14 P. Chmielarz, *Polym. Adv. Technol.*, 2018, **29**, 470–480.
15 P. Chmielarz, *Polimery*, 2021, **62**, 642–649.
16 P. Chmielarz, *Polym. Adv. Technol.*, 2017, **28**, 1787–1793.
17 E. Trevisanello, F. De Bon, G. Daniel, F. Lorandi, C. Durante, A. A. Isse and A. Gennaro, *Electrochim. Acta*, 2018, **285**, 344–354.
18 Y. Sun, S. Lathwal, Y. Wang, L. Fu, M. Olszewski, M. Fantin, A. E. Enciso, G. Szczepaniak, S. Das and K. Matyjaszewski, *ACS Macro Lett.*, 2019, **8**, 603–609.
19 T. Wu, E. R. Lankshear and A. J. Downard, *Chemelectrochem*, 2019, **6**, 5149–5154.
20 D. Li, J. Y. Wu, S. Y. Yang, W. J. Zhang, X. Q. Niu, Y. H. Chen and F. Ran, *New J. Chem.*, 2018, **42**, 2692–2701.
21 I. Zaborniak, A. Macior and P. Chmielarz, *Materials*, 2020, 13.
22 I. Zaborniak, P. Chmielarz, M. R. Martinez, K. Wolski, Z. Y. Wang and K. Matyjaszewski, *Eur. Polym. J.*, 2020, 126.
23 F. De Bon, S. Marenzi, A. A. Isse, C. Durante and A. Gennaro, *Chemelectrochem*, 2020, **7**, 1378–1388.
24 B. Y. Zhao, M. Mohammed, B. A. Jones and P. Wilson, *Chem. Commun.*, 2021, **57**, 3897–3900.
25 M. Fantin, S. Park, Y. Wang and K. Matyjaszewski, *Macromolecules*, 2016, **49**, 8838–8847.
26 M. Fantin, P. Chmielarz, Y. Wang, F. Lorandi, A. A. Isse, A. Gennaro and K. Matyjaszewski, *Macromolecules*, 2017, **50**, 3726–3732.
27 I. Zaborniak and P. Chmielarz, *Polym. Adv. Technol.*, 2020, **31**, 2806–2815.
28 P. Chmielarz, J. J. Yan, P. Krys, Y. Wang, Z. Y. Wang, M. R. Bockstaller and K. Matyjaszewski, *Macromolecules*, 2017, **50**, 4151–4159.
29 N. Shida, Y. Koizumi, H. Nishiyama, I. Tomita and S. Inagi, *Angew. Chem., Int. Ed.*, 2015, **54**, 3922–3926.
30 B. Li, B. Yu, W. T. S. Huck, W. Liu and F. Zhou, *J. Am. Chem. Soc.*, 2013, **135**, 1708–1710.
31 P. Chmielarz, P. Krys, Z. Wang, Y. Wang and K. Matyjaszewski, *Macromol. Chem. Phys.*, 2017, **218**, 1700106.
32 B. Li, B. Yu, W. T. S. Huck, F. Zhou and W. Liu, *Angew. Chem., Int. Ed.*, 2012, **51**, 5092–5095.
33 S. Park, P. Chmielarz, A. Gennaro and K. Matyjaszewski, *Angew. Chem., Int. Ed.*, 2015, **54**, 2388–2392.
34 F. Lorandi, M. Fantin, A. A. Isse and A. Gennaro, *Polym. Chem.*, 2016, **7**, 5357–5365.
35 M. Fantin, A. A. Isse, A. Gennaro and K. Matyjaszewski, *Macromolecules*, 2015, **48**, 6862–6875.
36 A. J. D. Magenau, N. Bortolamei, E. Frick, S. Park, A. Gennaro and K. Matyjaszewski, *Macromolecules*, 2013, **46**, 4346–4353.
37 J.-K. Guo, Y.-N. Zhou and Z.-H. Luo, *AIChE J.*, 2015, **61**, 4347–4357.
38 W. Tang, Y. Kwak, W. Braunecker, N. V. Tsarevsky, M. L. Coote and K. Matyjaszewski, *J. Am. Chem. Soc.*, 2008, **130**, 10702–10713.
39 A. A. Isse, F. Lorandi and A. Gennaro, *Curr. Opin. Electrochem.*, 2019, **15**, 50–57.
40 F. Lorandi, M. Fantin, A. A. Isse, A. Gennaro and K. Matyjaszewski, *Electrochim. Acta*, 2018, **260**, 648–655.

41 W. A. Braunecker, N. V. Tsarevsky, A. Gennaro and K. Matyjaszewski, *Macromolecules*, 2009, **42**, 6348–6360.
42 M. Fantin, A. A. Isse, K. Matyjaszewski and A. Gennaro, *Macromolecules*, 2017, **50**, 2696–2705.
43 G. R. Jones, A. Anastasaki, R. Whitfield, N. Engelis, E. Liarou and D. M. Haddleton, *Angew. Chem., Int. Ed.*, 2018, **57**, 10468–10482.
44 S. Perrier, S. P. Armes, X. S. Wang, F. Malet and D. M. Haddleton, *J. Polym. Sci. Part A: Polym. Chem.*, 2001, **39**, 1696–1707.
45 X. S. Wang, F. L. G. Malet, S. P. Armes, D. M. Haddleton and S. Perrier, *Macromolecules*, 2001, **34**, 162–164.
46 S. Perrier and D. M. Haddleton, *Macromol. Symp.*, 2002, **182**, 261–272.
47 Y. Li, S. P. Armes, X. Jin and S. Zhu, *Macromolecules*, 2003, **36**, 8268–8275.
48 S. B. Lee, A. J. Russell and K. Matyjaszewski, *Biomacromolecules*, 2003, **4**, 1386–1393.
49 N. V. Tsarevsky, T. Pintauer and K. Matyjaszewski, *Macromolecules*, 2004, **37**, 9768–9778.
50 E. E. Oseland, Z. J. Ayres, A. Basile, D. M. Haddleton, P. Wilson and P. R. Unwin, *Chem. Commun.*, 2016, **52**, 9929–9932.
51 S. Dadashi-Silab, I.-H. Lee, A. Anastasaki, F. Lorandi, B. Narupai, N. D. Dolinski, M. L. Allegrezza, M. Fantin, D. Konkolewicz, C. J. Hawker and K. Matyjaszewski, *Macromolecules*, 2020, **53**, 5280–5288.
52 M. G. Fraser, H. van der Salm, S. A. Cameron, A. G. Blackman and K. C. Gordon, *Inorg. Chem.*, 2013, **52**, 2980–2992.
53 K. Parkatzidis, H. S. Wang, N. P. Truong and A. Anastasaki, *Chem*, 2020, **6**, 1575–1588.